INORGANIC CHEMISTRY
FRONTIERS

RESEARCH ARTICLE

View Article Online
View Journal | View Issue

Cite this: *Inorg. Chem. Front.*, 2023, **10**, 118

Towards panchromatic Fe(II) NHC sensitizers *via* HOMO inversion†

Anil Reddy Marri, [a,b] Bogdan Marekha, [c,d] Thomas Penfold, [e] Stefan Haacke *[c] and Philippe C. Gros *[a]

Received 2nd September 2022,
Accepted 10th November 2022

DOI: 10.1039/d2qi01903e

rsc.li/frontiers-inorganic

A combined experimental and theoretical study of iron(II) complexes with pyridyl N-heterocyclic carbene ligands is presented, with a new focus on the effect of extending the ligands with thiophenes of variable number. In agreement with recent theoretical predictions by the Jakubikova group, these ligands induce a substantial mixture of the occupied t_{2g} and π HOMO orbitals, as manifested by a near 80 nm red-shift of the ^{1}MLCT transition and a 2–3 fold increase of the molar extinction coefficient. The thiophene moieties permit delocalisation of the MLCT state on the ligands, which results in excited state lifetimes in the 13–18 ps range, almost twice as much as for the reference compound lacking the thienyl substituents. Relaxation into ^{3}MC states remains the main ^{3}MLCT quenching mechanism, and the effect of the number of thiophenes in lengthening the ^{3}MLCT lifetime is qualitatively consistent with a reduction in the ^{3}MLCT–^{3}MC energy gap.

Introduction

The replacement of noble metals by earth-abundant substitutes is at the forefront of current research[1–4] aimed at developing sustainable photoactive materials required for solar energy conversion or photocatalysis. Iron is by far the most abundant metal in Earth's crust and appears a promising candidate to replace the ruthenium gold standard that is in the same column of the periodic table.

Ruthenium polypyridine complexes have been applied extensively for sensitization in Dye-sensitized solar cells (DSSCs).[5–10] Their photophysical and redox properties facilitate efficient light harvesting through long-lived Metal-to-Ligand Charge Transfer (MLCT) states which are responsible for electron transfer into semiconductors and efficient ground state regeneration after excitation.[11–13]

In contrast Fe(II)-polypyridines have short-lived MLCT states due to an ultrafast intersystem crossing populating their low-lying metal centred (MC) states.[14–17] To date increasing the ligand field strength has been the strategy of choice to increase the energy of the unreactive low-lying ligand field states. Ligands based on σ-donating NHC (N-heterocyclic carbenes). The MLCT lifetime has reached tens of picoseconds for complexes with tridentate C^N^C[18–20] and bidentate C^N ligands,[21–24] and nanoseconds for compounds bearing tridentate C^C^C ligands,[25] making it possible for iron to be used in photochemical applications such as iron-sensitized DSSCs.[26–31] However, apart from the recently published Fe(II) complex with phenN,N′^C ligands,[32] this improvement in lifetime was obtained at the sacrifice of achieving the panchromatic absorption required for solar energy conversion applications. Recently, "HOMO inversion" has emerged as a promising concept in the field.[33–35] This approach aims to adjust the filled orbital energetic levels in order to mix metal t_{2g} and ligand molecular orbitals thus switching the HOMO localization from the metal to the ligand (Fig. 1). This approach was demonstrated experimentally by the Herbert group[35] to design new panchromatic iron(II) complexes using ligands combining amido donors with benzannulated phenanthridine and quinoline. The covalent amido–Fe bond deeply strengthened the

[a]*Université de Lorraine, CNRS, L2CM, F-54000 Nancy, France. E-mail: philippe.gros@univ-lorraine.fr*
[b]*Department of Chemistry, North Carolina State University, 851 Main Campus Drive, Raleigh, North Carolina, 27695-8204, USA*
[c]*Université de Strasbourg, CNRS, IPCMS, F-67000 Strasbourg, France*
[d]*Max-Planck-Institute for Medical Research, D-69120 Heidelberg, Germany*
[e]*Chemistry-School of Nat. & Env. Sci., Newcastle University, Newcastle Upon-Tyne, UK*

†Electronic supplementary information (ESI) available. See DOI: https://doi.org/10.1039/d2qi01903e

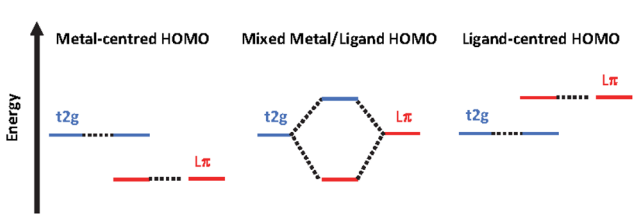

Fig. 1 Energetic diagrams illustrating the HOMO inversion concept.

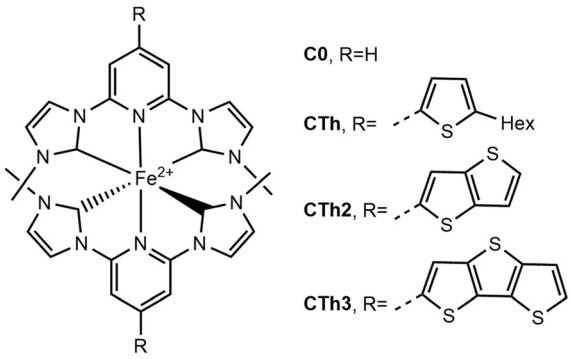

Fig. 2 Complexes studied in this work. The counterion is PF_6^- throughout.

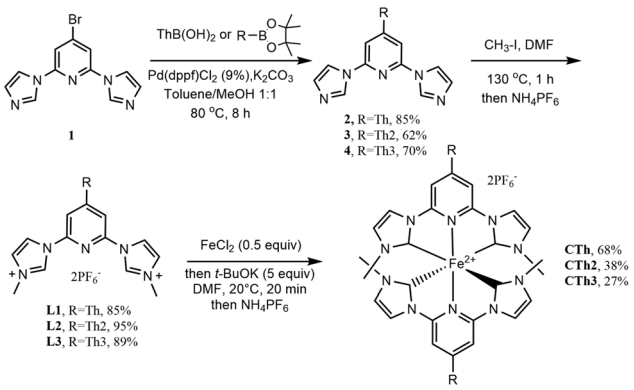

Scheme 1 Synthesis of ligand precursors and thienyl substituted complexes.

ligand field subsequently producing long lived excited states with up to 2.5 ns lifetime.

The group of E. Jakubikova[33] has reported a computational work on a series of iron(II) polypyridine complexes and predicted that the ligand π-delocalization should promote notable changes in absorption features and suggested that the same effect could be expected with pyridylNHC Fe(II) complexes. To our knowledge besides this exclusively computational work, the effect of π-delocalization and the impact of HOMO inversion on the photophysical and electronic properties of pyridylNHC Fe(II) complexes has not been investigated yet.

Herein we report the synthesis of complexes **CTh**, **CTh2** and **CTh3** designed with thiophene and fused polythiophenes conjugated with the central pyridine ring of the pyridylNHC ligand (Fig. 2) and the investigation of their photophysical properties by means of ultra-fast transient absorption. Complex **C0** is the proto-typical $[Fe(bmip)_2]^{2+}$, where bmip = 2,6-bis(3-methyl-imidazole-1-ylidine)-pyridine, published by the group of Wärnmark.[18,36] We demonstrate that, as compared to **C0**, extending the delocalization promotes an important red-shift of the pyridine-MLCT absorption band and an impressive increase of the molar extinction coefficients. The excited state lifetimes were also increased substantially by comparison with the unsubstituted complexes while they were slightly impacted by the conjugation extent.

Results and discussion

Synthesis of ligands and complexes

The imidazolium salts **L1**, **L2** and **L3**, that are the required precursors of the pyridyl-NHC ligands to be coordinated to iron, were first synthesized (Scheme 1, see ESI† for experimental details). **L1** was obtained following our reported procedure.[27] **L2** and **L3** were obtained in good yields respectively by quaternization of pyridylimidazoles **3** and **4** resulting from a Suzuki coupling of the bromo derivative **1** [27] with the appropriate preformed thienyl boron pinacol esters that were obtained by a lithiation–borylation sequence on the parent thienyl compounds (see ESI†).[37,38] The target complexes were finally obtained in good to moderate yield applying an *in situ* coordination protocol. $FeCl_2$ was first reacted with the appropriate ligand precursor, then *t*-BuOK was added to generate the carbene moiety. The coordination yield was found dependent on the number of thiophenes attached to the central pyridine. This agrees with the weakening of the pyridine nitrogen coordination ability by conjugation with the extended π-system.

Electronic properties of complexes

The UV-Vis absorption spectra of the three complexes in deaerated acetonitrile solution are shown in Fig. 3 and the data concerning the lowest energy bands are collected in Table 1. The complexes display three distinct absorption bands. The band at higher energy (250–350 nm) is assigned to ligand-centered π–π* transitions, while the two other bands at lower energy, correspond to Fe-NHC transitions (340–420 nm) and Fe-pyri-

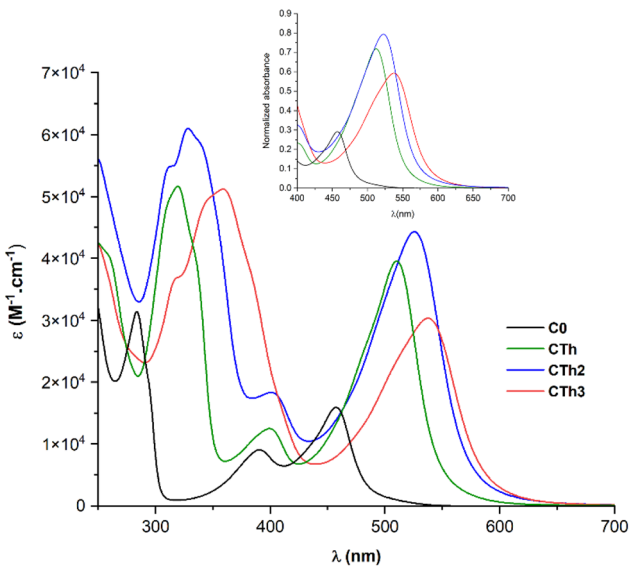

Fig. 3 UV-Vis spectra of complexes in acetonitrile. Inset: normalized absorbance for the lowest energy band.

Table 1 Spectroscopic and electrochemical properties of complexes

Complex	λ_{max} (nm) (ε(M^{-1} cm^{-1}))	E_{ox} (Fe^{II}/Fe^{III}) (V SCE^{-1})	E_{Red} (V SCE^{-1})	ΔE
C0 [18,22]	284 (31 433) 390 (9077) 457 (15 955)	0.80 (rev)	−1.95 (irr)	2.75
CTh	319 (51 619) 399 (12 519) 516 (39 330)	0.68 (rev)	−1.69 (qr)	2.37
CTh2	328 (61 027) 401 (18 354) 526 (44 300)	0.71 (rev)	−1.56 (qr)	2.27
CTh3	359 (51 200) 535 (30 240)	0.73 (rev)	−1.52 (irr)	2.25

dine MLCT transitions (410–650 nm). In **CTh3**, the very broad π–π* absorption band of the dithienothiophene moiety masks the Fe-NHC MLCT band.

As a general trend, the substitution of complex **C0** with thiophenes promoted a notable bathochromic effect on both the π–π* and Fe-pyridine MLCT bands and the amplitude of the red-shift was directly related to the number of thiophene units ($\Delta\lambda$ = 78 nm going from **C0** to **CTh3**). In contrast, the thiophenes had no impact on the Fe-carbene MLCT band the transition energy of which remained constant.

Focusing on the lowest-energy portion of the spectrum, the MLCT Fe-pyridine band, **CTh**, **CTh2** and **CTh3** present a broad and intense absorption, ranging from 450 to 620 nm. Among all, **CTh3** showed the broadest and most red shifted absorption (535 nm, ε = 30 240 M^{-1} cm^{-1}) and **CTh2** the highest extinction coefficient (526 nm, ε = 44 300 M^{-1} cm^{-1}).

The cyclic voltammetry data (Table 1) globally confirm the UV-Vis absorption spectroscopy results. The electrochemical gap markedly decreased when comparing **CTh** to **C0** in agreement with the 59 nm redshift of the MLCT band upon addition of one thiophene unit on the central pyridine. Also corroborating the absorption spectra, a decrease of the gap was observed albeit in a lesser extent going from **CTh** to **CTh3**.

Table 2 gathers the computed energy and oscillator strengths for the lowest singlet excited states of **C0**, **CTh**, **CTh2** and **CTh3** that are associated with the lowest band in the absorption spectrum. Consistent with the experimental observations, a red shift of the lowest transitions of **CTh**, **CTh2** and **CTh3** compared to **C0** is observed and this increases with the delocalization of the MLCT state. The HOMO–LUMO gap is slightly larger than experimentally measured, but exhibits the same trend as the cyclic voltammetry data in Table 1.

Table 2 Computed energies of the HOMO and LUMO energies and lowest singlet excited states of **C0**, **CTh**, **CTh2** and **CTh3** calculated at the ground state optimized geometry using TDDFT(B3LYP*)

Complex	λ (nm) (f)	ε_{HOMO}/eV	ε_{LUMO}/eV	ΔE/eV
C0	518 (0.00163) 518 (0.00162)	−5.33	−2.02	3.31
CTh	615 (0.00340) 614 (0.00370)	−5.29	−2.41	2.88
CTh2	628 (0.00290) 627 (0.00260)	−5.32	−2.56	2.76
CTh3	637 (0.00430) 637 (0.00340)	−5.33	−2.62	2.71

The HOMO and LUMO have been plotted for all the complexes (Fig. 4 and ESI†). Fig. 4 clearly evidenced a significant enhancement of the mixing between the ligand and metal orbitals in the HOMO as the thiophene units are included. The Fe 3d orbitals contribution to the HOMO decreased with the increase of the number of thienyl units in the substituent.

Excited state dynamics and relaxation

Temporal evolution of the fs-TAS signal of the **CTh** series of molecules bears a number of common features and therefore will be illustrated on the example of **CTh3** (Fig. 5, see the ESI† for data on the other molecules). In particular, upon optical excitation of the Fe-pyridine MLCT transition by the pump pulse the differential transient spectra in the 360–680 nm spectral range reveal two negative and two positive features. The former ones (<390 nm, 500–580 nm) come from the depletion of the population of the initial state (ground state bleaching, GSB) and peak around the absorption maxima of the Fe-pyridine and Fe-NHC MLCT transitions (Fig. 5B). In turn, the positive features originate from the excited state absorption (ESA) of the states populated by the pump pulse. Notably, the high-energy ESA (400–470 nm) shows twice the intensity of the low energy ESA feature (>580 nm).

The initially observed spectral features exhibit an ultrafast evolution on the sub-200 fs time scale. Namely, the high-energy ESA undergoes a pronounced blue-shift, which is most evident by the zero-crossing point moving from 500 nm at 0 ps to ~475 nm at 200 fs (Fig. 5B and 480 nm trace in Fig. 5C). The low-energy ESA shows similar development. Also, a somewhat delayed rise of the low-energy GSB band suggests that it overlaps with the ultrafast evolving ESA. Further temporal evol-

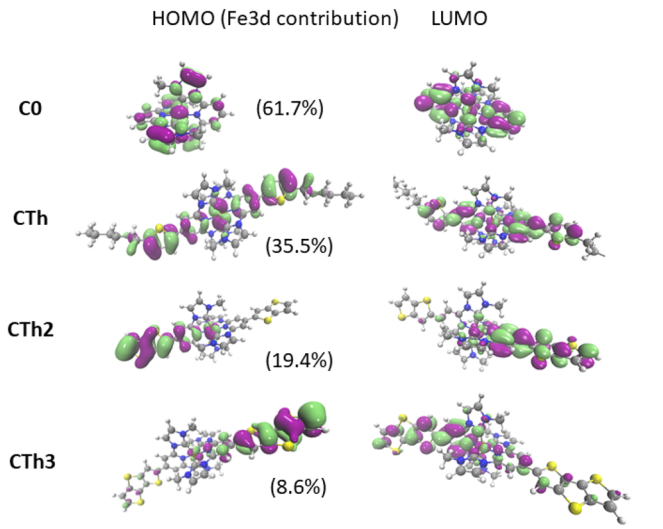

Fig. 4 HOMO–LUMO plots for all the complexes including the contribution of Fe 3d orbitals in HOMO.

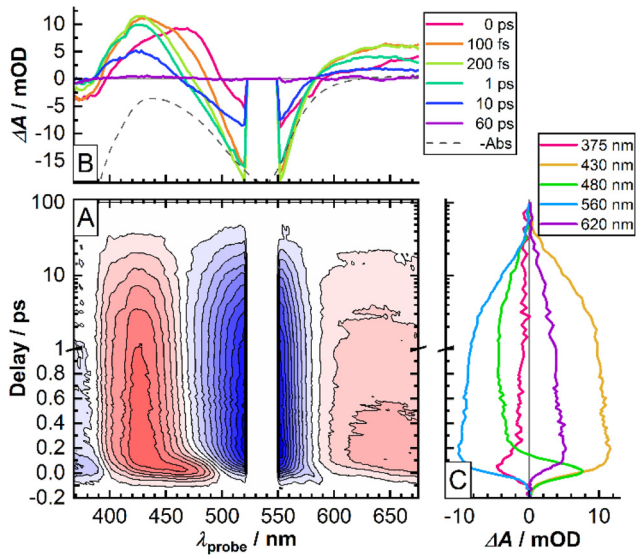

Fig. 5 Fs-TAS data for **CTh3**. (A) Two-dimensional color-plot as a function of pump–probe delay and probe wavelength. Positive signals (induced absorption) are in shades of red, whereas negative ones (bleach) are in shades of blue. Contour lines are drawn at 10% intervals of the absolute maximum value. The data around 535 ± 10 nm were omitted due to large noise of scattered pump light overlaying the TAS signal. The time axis is logarithmic above 1 ps delay. (B) Transient spectra at selected delays. Inverse-signed steady-state UV-vis absorption spectrum is shown for comparison (dashed line). (C) Kinetic traces at selected probe wavelengths.

ution shows little spectral variation and rather reflects intensity decay on the ~15 ps time scale. The ESA and GSB features decay concomitantly thereby evidencing complete relaxation of the excited state population back to the ground state.

To provide a quantitative framework to the observed fs-TAS results and given the concerted nature of temporal evolution of different transient spectral features, we performed a global analysis[39] using GloTarAn software[40] assuming a sequential decay model convoluted with a Gaussian instrument response function (IRF). The data could be satisfactorily described by a sum of 4 exponential functions (see the ESI† for the discussion on the relevance of the 4th exponential function). The corresponding decay time constants are reported in Table 3 and the evolution associated difference spectra (EADS) for **CTh3** are shown in Fig. 6.

In accordance with the qualitative analysis of the experimental data, the first sub-100 fs component revealed by the global analysis accounts for the initial blue-shift of both high

Table 3 Time constants derived from the analysis of the TAS data[a]

	CTh	CTh2	CTh3
τ_1 (ps)	<0.01	0.030	0.045
τ_2 (ps)	0.17	0.21	0.43
τ_3 (ps)	3.0	4.7	5.2
τ_4 (ps)	13.2	15.5	17.9

[a] For the reference complex **C0**, τ_4 is 9 ps.[18,36]

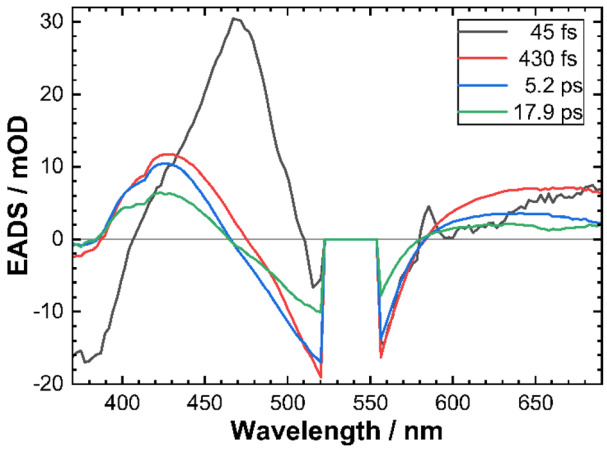

Fig. 6 Evolution associated difference spectra (EADS) obtained from global analysis of **CTh3** fs-TAS data. The corresponding decay time constants are indicated in the legend.

and low-energy ESA bands. The corresponding spectral profile of EADS also suggests that the high-energy part of the ESA feature is very intense as it largely compensates the GSB signal around the pump wavelength. The other sub-ps component bears some residual features of this transient blue-shift of the high energy ESA and corresponds to a significant part of the intensity decay of the low energy ESA on a sub-picosecond time scale (Fig. 5B). The two slower components mostly reveal the complete intensity decay back to the ground state with very little changes in band shape.

The physical picture of the photodynamics of these molecules upon MLCT optical excitation that emerges from these results resembles previous results from us[19,20,41–43] and others[18,44] on similar tridentate complexes with 4 NHC ligands. Namely, the initially created ^{1}MLCT state is converted through an ultrafast (<100 fs) spin-crossover to a hot non-emissive (no noticeable stimulated emission observed) ^{3}MLCT state which then undergoes a sub-ps vibrational relaxation. This thermalized triplet state then returns to the ground state on the ps time-scale. In particular the last, τ_4 ~ 18 ps, step corresponds to the return to the ground state, involving ultrafast relaxation through lower energy ^{3}MC states, in accordance with the relaxation cascade observed for the parent pyridylNHC Fe (II) complexes.[18,19,41–43] In particular the reference complex **C0** was studied in detail,[18,36] demonstrating a 9.0 ps lifetime of the ^{3}MLCT state (corresponding to τ_4).

The τ_3 = 5.2 ps is a relevant time constant since it is needed for an improved quality of the fits, in particular in the low energy bleach part (see Fig. S18†). However, unlike the 0.43 ps component, its EADS does not show a significant difference in spectral shape with the 17.9 ps EADS, unlike similar time components we found in previous work with diazinyl-NHC ligands.[20] This suggests two alternatives for its assignment. It could be due to a residual slower thermalization process which involves vibrational modes that are less strongly coupled to the optical transitions and which therefore leads to little spectral variation. Alternatively, τ_3 and τ_4 may correspond

to two different ^{3}MLCT–^{3}MC relaxation pathways in the multi-dimensional excited state landscape. As a side remark, a parallel population of both ^{3}MLCT and ^{3}MC on the sub-picosecond time scale[36,43,45] cannot be excluded, since population of the latter states go commonly un-noticed in UV-VIS transient absorption experiments.[42]

Concerning the influence of the number of fused thiophene rings in the **CTh** series of molecules on the excited state dynamics one can see from the results of the global analysis (Table 3) as well from the bleach recovery kinetics (Fig. 7) that increasing the number of fused thiophene rings and thereby promoting the electron delocalization in the MLCT state leads to a moderate slow-down of all the steps of the excited state relaxation. Nonetheless, this delocalization effect is apparently not enough to alter the overall relaxation cascade mechanism observed for related Fe-NHC complexes.

A Jablonski diagram showing the computed energetics of the key states for the series of complexes is shown in Fig. 8. While the MLCT states show a distinct red shift, the ^{3}MC states, which mix very little with the fused thiophene units (see spin density in Fig. S20†) remain largely unchanged among the **CTh**, **CTh2** and **CTh3** series compared to **C0**. The geometry of all the important structures are provided in the ESI.†

Given the significant structural reorganization between the ^{3}MLCT and ^{3}MC states, the decreasing energy gap (ΔE) between the two states as the number of thiophene units is increased may introduce a small barrier to the transformation between the two states, responsible for the increase in τ_3 and τ_4 observed experimentally. This counterintuitive effect is highlighted in Fig. 9. Indeed, and as in Marcus theory for electron transfer,[46] the energy barrier between the states decreases, and

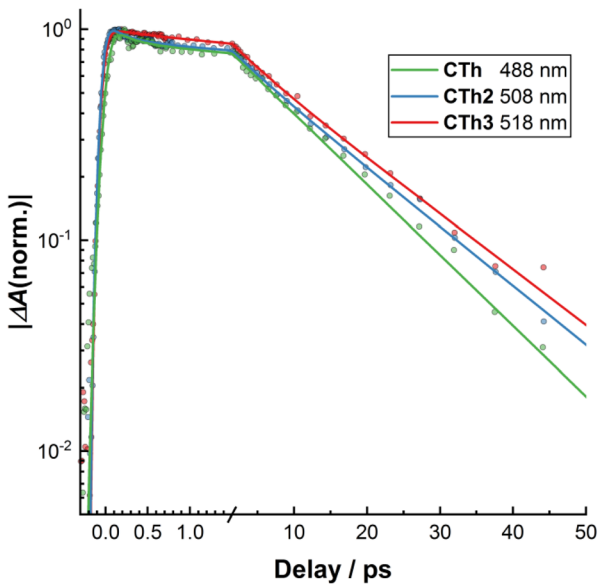

Fig. 7 Semi-log plot of normalized kinetics of the bleach recovery of **CTh**, **CTh2** and **CTh3**. Dots are measured datapoints whereas lines are results of the global fit (see text).

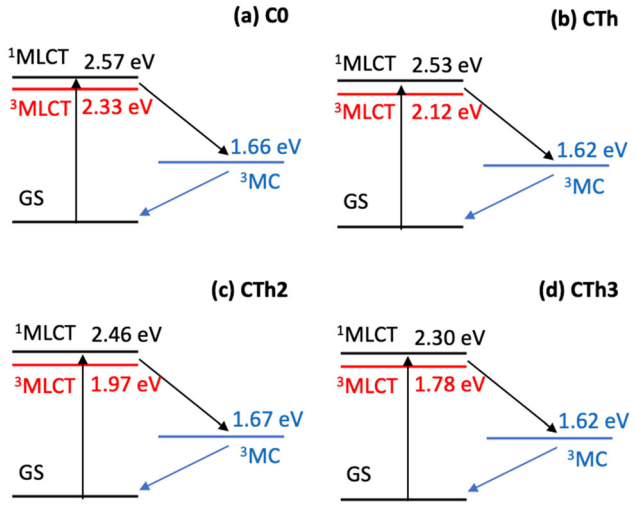

Fig. 8 Computed Jablonski diagrams of the important excited states in (a) **C0**, (b) **CTh**, (c) **CTh2** and (d) **CTh3**. Using TDDFT, the energies of the ^{1,3}MLCT states were computed at the ^{3}MLCT optimized geometry and the energies of the ^{3}MC was computed at the ^{3}MC optimized geometry (^{1}MLCT and ^{3}MLCT states have similar geometries). Both geometries were computed using UKS and the relevant geometries are in the ESI.†

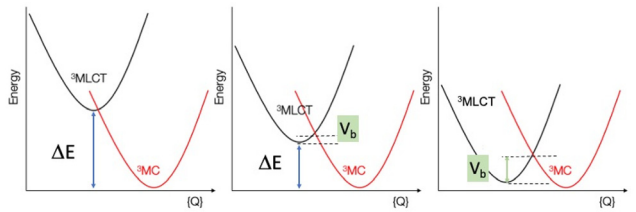

Fig. 9 Schematic representation of the ^{3}MLCT and the ^{3}MC states approximated as harmonic potentials along an effective structural coordinate Q. When the energy gap ΔE decreases (left to right), the barrier V_b between ^{3}MLCT and ^{3}MC increases, leading to a longer ^{3}MLCT lifetime.

reaches zero only when ΔE is equal to the structural reorganization energy. A similar behavior was recently also put forward in a study on solvent effects of Fe complexes.[47]

Conclusions

In conclusion, we present here a combined experimental and theoretical study of iron(II) complexes with pyridyl NHC ligands conjugated with thiophene and fused polythiophenes. As predicted theoretically,[33] these ligands induce a substantial mixture of the occupied t_{2g} and π HOMO orbitals, as manifested by a near 80 nm red-shift of the ^{1}MLCT transition and a 2–3-fold increase of the extinction coefficient. The thiophene moieties allow for a delocalisation of the MLCT state on the ligands, which results in excited state lifetimes in the 13–18 ps range, almost twice as much as for the reference compound lacking the thiophene side groups. Relaxation into ^{3}MC states remains the main ^{3}MLCT quenching mechanism, and the

effect of the number of thiophenes in lengthening the ^{3}MLCT lifetime is qualitatively consistent with a stabilisation of the ^{3}MLCT energy due to increased charge delocalisation. As a result, the ^{3}MLCT–^{3}MC energy gap is reduced (Fig. 8), which leads to an increased barrier for the excited state structural relaxation involved in the ^{3}MLCT–^{3}MC transition (Fig. 9). Works are in progress to further amplify the mixing between metal and ligand orbitals *via* a wider π-extended delocalization in various parts of the ligands.

Experimental

General

Solvents and commercially available reagents were used as received. Thin layer chromatography (TLC) was performed by using silica gel 60 F-254 (Merck) plates and visualized under UV light. Chromatographic purification was performed by using silica gel 60 (0.063–0.2 mm per 70–230 mesh). ^{1}H (400 MHz) and ^{13}C NMR (100 MHz) spectra were taken on a DRX400 Bruker spectrometer at ambient temperature. The chemical shifts (δ), were calibrated by using either tetramethylsilane (TMS) or signals from the residual protons of the deuterated solvents and are reported in parts per million (ppm) from low to high field, NMR signal assignments for **L2**, **L3**, **CTh**, **CTh2** and **CTh3** are detailed in the ESI.†

High-resolution mass spectrometry (HRMS) data was obtained by using Bruker micrOTOF-Q spectrometer. UV-vis spectra were recorded in a 1 cm path length quartz cell on a LAMBDA 1050 (PerkinElmer), spectrophotometer. Cyclic voltammetry was performed on a Radiometer PST006 potentiostat using a conventional three-electrode cell. The saturated calomel electrode (SCE) was separated from the test compartment using a bridge tube. The solutions of studied complexes (0.2 mM) were purged with argon before each measurement. The test solution was acetonitrile containing 0.1 M Bu_4NPF_6 as supporting electrolyte. The working electrode was a vitreous carbon rod (1 cm^2) wire and the counter-electrode was a 1 cm^2 Pt disc. After the measurement, ferrocene was added as the internal reference for calibration. All potentials were quoted *versus* SCE. In these conditions the redox potential of the couple Fc^+/Fc was found at 0.39 V. In all the experiments the scan rate was 100 mV s^{-1}.

Synthesis of complexes

CTh. To an Ar degassed solution of **L1**[27] (88 mg, 0.126 mmol) in 2 mL of anhydrous DMF was added anhydrous $FeCl_2$ (8 mg, 0.063 mmol). Then *t*-BuOK (0.071 g, 0.630 mmol) was added to the above mixture and stirred at room temperature for 20 min. A saturated aqueous solution of NH_4PF_6 was added (10 ml) and the precipitate was collected by filtration. The crude product was further purified by silica gel column chromatography eluting with an acetone/H_2O/KNO_3(sat) = 10/3/0.5 mixture. The reddish fraction was collected and after evaporation of acetone, the left solution was treated with a saturated solution of NH_4PF_6. The desired complex precipitate was then filtered, washed with distilled water followed by ether, and dried under vacuum. **CTh** was obtained as a reddish solid (50 mg, 68% yield). ^{1}H NMR (400 MHz, CD_3CN, δ ppm): 8.12 (d, J = 2.19 Hz, 2H), 7.95 (s, 2H), 7.84 (d, J = 3.72 Hz, 1H), 7.06 (s, J = 3.72 Hz, 1H), 7.04 (d, J = 2.19 Hz, 2H), 2.99 (t, J = 7.51 Hz, 2H), 2.62 (s, 6H), 1.79 (q, 2H), 148–1.35 (m, 6H), 0.95 (t, J = 7.09 Hz, 3H). ^{13}C NMR (100 MHz, CD_3CN, δ ppm): 201.1, 154.5, 151.4, 144.5, 138.0, 128.7, 127.2, 127.0, 116.1, 101.6, 35.3, 32.0, 31.8, 30.5, 29.0, 22.9, 14.0. ESI-HRMS calcd for $C_{46}H_{54}FeN_{10}S_2$ m/z = 433.1656. Found: 433.1653 [M − $2PF_6$].

CTh2. The same procedure was repeated using **L2** (80 mg, 0.119 mmol), $FeCl_2$ (8 mg, 0.06 mmol) and *t*-BuOK (68 mg, 0.597 mmol). **CTh2** was obtained as a purple solid (50 mg, 38% yield). ^{1}H NMR (400 MHz, CD_3CN, δ ppm): 8.26 (s, 1H), 8.17(d, J = 2.10 Hz, 2H), 8.05(s, 2H), 7.76(d, J = 5.30 Hz, 1H), 7.52(d, J = 5.28 Hz, 1H), 7.05(d, J = 2.10 Hz, 2H), 2.64(s, 6H). ^{13}C NMR (100 MHz, CD_3CN, δ ppm): 200.8, 154.6, 144.6, 142.2, 141.7, 141.0, 131.7, 127.1, 120.9, 120.7, 117.1, 101.9, 35.3. ESI-HRMS calcd for $C_{38}H_{30}FeN_{10}S_4$ m/z = 405.0438. Found: 405.0493 [M − $2PF_6$].

CTh3. The same procedure was repeated using **L3** (57 mg, 0.079 mmol), $FeCl_2$ (5 mg, 0.039 mmol) and *t*-BuOK (44 mg, 0.392 mmol). **CTh3** was obtained as a purple solid (13 mg, 27% yield). ^{1}H NMR (400 MHz, CD_3CN, δ ppm): 8.30 (s, 1H), 8.17 (d, J = 2.12 Hz, 2H), 8.06 (s, 2H), 7.71 (d, J = 5.29 Hz, 1H), 7.53 (d, J = 5.30 Hz, 1H), 7.06 (d, J = 2.09 Hz, 2H), 2.65 (s, 6H). ^{13}C NMR (100 MHz, CD_3CN, δ ppm): 200.8, 154.6, 144.5, 144.2, 143.3, 140.8, 133.1, 131.2, 129.7, 127.2, 122.4, 122.0, 117.1, 101.8, 35.3. ESI-HRMS calcd for $C_{42}H_{30}FeN_{10}S_6$ m/z = 461.0159. Found: 461.0175 [M − $2PF_6$].

Computational details

All complexes were optimized in the ground state and ^{3}MC and ^{3}MLCT states using DFT within the approximation of the B3LYP* exchange and correlation functional[48] and a def2-SVP basis set[49] as implemented within the ORCA quantum chemistry package.[50] While this is only valid for the lowest state of each multiplicity, both the ^{3}MC and ^{3}MLCT are the lowest triplets at their respective optimized geometries. Numerical frequencies calculations were carried out on the geometries optimized to ensure no negative frequencies. TDDFT calculations, used to calculate the excited state energies of each complex used the Tamm–Dancoff approximation[51] and were also performed using B3LYP*. All simulations were performed using a polarisable continuum model with the parameters of acetonitrile.

Fs-TAS measurements

The home-built transient absorption spectrometer has been described in detail elsewhere[52,53] and only substantial parameters will be given here. The pump pulses were tuned to be in resonance with the absorption maxima of the studied compounds (510 nm for **CTh**, 525 nm for **CTh2** and 535 nm for **CTh3**). The probe light covering 360–700 nm range was generated by focusing 40 fs 800 nm pulses of the primary laser

source in a 2 mm thick CaF_2 plate mounted on a motorized linear stage to reduce thermal effects. Sample solutions (1 mM in dry acetonitrile) were circulated in a flow cell with 200 μm optical pathlength (Starna). The probe beam was focused to *ca.* 60 μm Gaussian spot diameter ($1/e^2$). The pump spot size was *ca.* 150 μm in diameter ($1/e^2$) and typical maximal energy densities were 0.25 mJ cm^{-2} (in the center of the Gaussian beam profile) to keep the fraction of excited molecules below 5%. Solvent subtraction and correction for wavelength-dependent time-zero were performed using previously established protocols[52,53] using the neat solvent data acquired under identical conditions.

Author contributions

A. R. M. performed the synthesis and ground state characterization of ligands and complexes. B. M. performed transient absorption spectroscopy experiments and analysed the results with S. H., T. P. performed DFT computations and analysed the results. P. C. G. conceived the project and wrote the manuscript with B. M., T. P. and S. H.

Conflicts of interest

There are no conflicts to declare.

Acknowledgements

The Strasbourg team is grateful to Dr O. Crégut for expert help in laser maintenance and development of data acquisition software, and for the funding provided by the ITI 2021–28 program of the University of Strasbourg, CNRS and Inserm, supported by IdEx Unistra (ANR 10 IDEX 0002), by SFRI STRAT'US project (ANR 20 SFRI 0012) and EUR QMAT ANR-17-EURE-0024 under the framework of the French Investments for the Future Program. The L2CM thanks the French Agence Nationale de Recherche (ANR-16-CE07-0013-02), Lorraine Université d'Excellence (IMPACT N4S) and the European Regional Development Funds (Programme opérationnel FEDER-FSE Lorraine et Massif des Vosges 2014-2020/"Fire Light" project: "Photo-bio-active molecules and nanoparticles" for financial support and grants to A. R. M. The L2CM also warmly thanks S. Parant for the electrochemical experiments and F. Dupire from the mass spectrometry MassLor platform of Lorraine. TJP acknowledges the EPSRC through grant EP/V010573/1 for support.

References

1 T. Duchanois, L. Liu, M. Pastore, A. Monari, C. Cebrián, Y. Trolez, M. Darari, K. Magra, A. Francés-Monerris, E. Domenichini, M. Beley, X. Assfeld, S. Haacke and P. Gros, NHC-Based Iron Sensitizers for DSSCs, *Inorganics*, 2018, **6**, 63.
2 O. S. Wenger, Photoactive Complexes with Earth-Abundant Metals, *J. Am. Chem. Soc.*, 2018, **140**, 13522–13533.
3 S. Kaufhold and K. Wärnmark, Design and Synthesis of Photoactive Iron N-Heterocyclic Carbene Complexes, *Catalysts*, 2020, **10**, 132.
4 P. Dierks, Y. Vukadinovic and M. Bauer, Photoactive iron complexes: more sustainable, but still a challenge, *Inorg. Chem. Front.*, 2022, **9**, 206–220.
5 B. O'Regan and M. Grätzel, A Low-Cost, High-Efficiency Solar Cell Based on Dye-Sensitized Colloidal TiO_2 Films, *Nature*, 1991, **353**, 737–740.
6 M. K. Nazeeruddin, A. Kay, I. Rodicio, R. Humphry-Baker, E. Mueller, P. Liska, N. Vlachopoulos and M. Graetzel, Conversion of light to electricity by cis-X2bis(2,2′-bipyridyl-4,4′-dicarboxylate)ruthenium(II) charge-transfer sensitizers (X=Cl-, Br-, I-, CN-, and SCN-) on nanocrystalline titanium dioxide electrodes, *J. Am. Chem. Soc.*, 1993, **115**, 6382–6390.
7 Md. K. Nazeeruddin, S. M. Zakeeruddin, J.-J. Lagref, P. Liska, P. Comte, C. Barolo, G. Viscardi, K. Schenk and M. Graetzel, Stepwise assembly of amphiphilic ruthenium sensitizers and their applications in dye-sensitized solar cell, *Coord. Chem. Rev.*, 2004, **248**, 1317–1328.
8 K. C. D. Robson, P. G. Bomben and C. P. Berlinguette, Cycloruthenated sensitizers: improving the dye-sensitized solar cell with classical inorganic chemistry principles, *Dalton Trans.*, 2012, **41**, 7814–7829.
9 M. G. Lobello, K.-L. Wu, M. A. Reddy, G. Marotta, M. Grätzel, M. K. Nazeeruddin, Y. Chi, M. Chandrasekharam, G. Vitillaro and F. De Angelis, Engineering of Ru(II) dyes for interfacial and light-harvesting optimization, *Dalton Trans.*, 2014, **43**, 2726–2732.
10 S. Mathew, A. Yella, P. Gao, R. Humphry-Baker, B. F. E. Curchod, N. Ashari-Astani, I. Tavernelli, U. Rothlisberger, Md. K. Nazeeruddin and M. Grätzel, Dye-sensitized solar cells with 13% efficiency achieved through the molecular engineering of porphyrin sensitizers, *Nat. Chem.*, 2014, **6**, 242–247.
11 S. Ardo and G. J. Meyer, Photodriven heterogeneous charge transfer with transition-metal compounds anchored to TiO_2 semiconductor surfaces, *Chem. Soc. Rev.*, 2009, **38**, 115–164.
12 A. Listorti, C. Creager, P. Sommeling, J. Kroon, E. Palomares, A. Fornelli, B. Breen, P. R. F. Barnes, J. R. Durrant, C. Law and B. O'Regan, The mechanism behind the beneficial effect of light soaking on injection efficiency and photocurrent in dye sensitized solar cells, *Energy Environ. Sci.*, 2011, **4**, 3494–3501.
13 A. Listorti, B. O'Regan and J. R. Durrant, Electron Transfer Dynamics in Dye-Sensitized Solar Cells, *Chem. Mater.*, 2011, **23**, 3381–3399.
14 J. E. Monat and J. K. McCusker, Femtosecond Excited-State Dynamics of an Iron(II) Polypyridyl Solar Cell Sensitizer Model, *J. Am. Chem. Soc.*, 2000, **122**, 4092–4097.

15 G. Auböck and M. Chergui, Sub-50 fs photoinduced spin crossover in $[Fe(bpy)_3]^{2+}$, *Nat. Chem.*, 2015, **7**, 629–633.
16 A. L. Smeigh, M. Creelman, R. A. Mathies and J. K. McCusker, Femtosecond Time-Resolved Optical and Raman Spectroscopy of Photoinduced Spin Crossover: Temporal Resolution of Low-to-High Spin Optical Switching, *J. Am. Chem. Soc.*, 2008, **130**, 14105–14107.
17 M. Cammarata, R. Bertoni, M. Lorenc, H. Cailleau, S. Di Matteo, C. Mauriac, S. F. Matar, H. Lemke, M. Chollet, S. Ravy, C. Laulhé, J.-F. Létard and E. Collet, Sequential Activation of Molecular Breathing and Bending during Spin-Crossover Photoswitching Revealed by Femtosecond Optical and X-Ray Absorption Spectroscopy, *Phys. Rev. Lett.*, 2014, **113**, 227402.
18 Y. Liu, T. Harlang, S. E. Canton, P. Chábera, K. Suárez-Alcántara, A. Fleckhaus, D. A. Vithanage, E. Göransson, A. Corani, R. Lomoth, V. Sundström and K. Wärnmark, Towards longer-lived metal-to-ligand charge transfer states of iron(II) complexes: an N-heterocyclic carbene approach, *Chem. Commun.*, 2013, **49**, 6412.
19 L. Liu, T. Duchanois, T. Etienne, A. Monari, M. Beley, X. Assfeld, S. Haacke and P. C. Gros, A new record excited state ^{3}MLCT lifetime for metalorganic iron(II) complexes, *Phys. Chem. Chem. Phys.*, 2016, **18**, 12550–12556.
20 M. Darari, E. Domenichini, A. Francés-Monerris, C. Cebrián, K. Magra, M. Beley, M. Pastore, A. Monari, X. Assfeld, S. Haacke and P. C. Gros, Iron(II) complexes with diazinyl-NHC ligands: impact of π-deficiency of the azine core on photophysical properties, *Dalton Trans.*, 2019, **48**, 10915–10926.
21 A. Francés-Monerris, K. Magra, M. Darari, C. Cebrián, M. Beley, E. Domenichini, S. Haacke, M. Pastore, X. Assfeld, P. C. Gros and A. Monari, Synthesis and Computational Study of a Pyridylcarbene Fe(II) Complex: Unexpected Effects of fac/mer Isomerism in Metal-to-Ligand Triplet Potential Energy Surfaces, *Inorg. Chem.*, 2018, **57**, 10431–10441.
22 K. Magra, E. Domenichini, A. Francés-Monerris, C. Cebrián, M. Beley, M. Darari, M. Pastore, A. Monari, X. Assfeld, S. Haacke and P. C. Gros, Impact of the fac/mer Isomerism on the Excited-State Dynamics of Pyridylcarbene Fe(II) Complexes, *Inorg. Chem.*, 2019, **58**, 5069–5081.
23 K. Magra, M. Darari, E. Domenichini, A. Francés-Monerris, C. Cebrián, M. Beley, M. Pastore, A. Monari, X. Assfeld, S. Haacke and P. C. Gros, Photophysical Investigation of Iron(II) Complexes Bearing Bidentate Annulated Isomeric Pyridine-NHC Ligands, *J. Phys. Chem. C*, 2020, **124**, 18379–18389.
24 K. Magra, A. Francés-Monerris, C. Cebrián, A. Monari, S. Haacke and P. C. Gros, Bidentate Pyridyl–NHC Ligands: Synthesis, Ground and Excited State Properties of Their Iron(II) Complexes and the Role of the fac/mer Isomerism, *Eur. J. Inorg. Chem.*, 2022, **7**, e202100818.
25 M. Bauer, J. Steube, A. Päpcke, O. Bokareva, T. Reuter, S. Demeshko, R. Schoch, S. Hohloch, F. Meyer, K. Heinze, O. Kühn and S. Lochbrunner, Janus-type dual emission of a Cyclometalated Iron(III) complex, *Research Square*, 2020, in review.
26 E. Marchini, M. Darari, L. Lazzarin, R. Boaretto, R. Argazzi, C. A. Bignozzi, P. C. Gros and S. Caramori, Recombination and regeneration dynamics in FeNHC (II)-sensitized solar cells, *Chem. Commun.*, 2020, **56**, 543–546.
27 A. Reddy Marri, E. Marchini, V. D. Cabanes, R. Argazzi, M. Pastore, S. Caramori and P. C. Gros, Record power conversion efficiencies for iron(II)-NHC-sensitized DSSCs from rational molecular engineering and electrolyte optimization, *J. Mater. Chem. A*, 2021, **9**, 3540–3554.
28 M. Becker, C. E. Housecroft and E. C. Constable, Electrolyte Tuning in Iron(II)-Based Dye-Sensitized Solar Cells: Different Ionic Liquids and I2 Concentrations, *Materials*, 2021, **14**, 3053.
29 M. Becker, V. Wyss, C. E. Housecroft and E. C. Constable, The influence of alkyl chains on the performance of DSCs employing iron(II) N-heterocyclic carbene sensitizers, *Dalton Trans.*, 2021, **50**, 16961–16969.
30 L. Lindh, O. Gordivska, S. Persson, H. Michaels, H. Fan, P. Chábera, N. W. Rosemann, A. K. Gupta, I. Benesperi, J. Uhlig, O. Prakash, E. Sheibani, K. S. Kjaer, G. Boschloo, A. Yartsev, M. Freitag, R. Lomoth, P. Persson and K. Wärnmark, Dye-sensitized solar cells based on Fe N-heterocyclic carbene photosensitizers with improved rod-like push-pull functionality, *Chem. Sci.*, 2021, **12**, 16035–16053.
31 A. R. Marri, E. Marchini, V. D. Cabanes, R. Argazzi, M. Pastore, S. Caramori, C. A. Bignozzi and P. C. Gros, A Series of Iron(II)–NHC Sensitizers with Remarkable Power Conversion Efficiency in Photoelectrochemical Cells, *Chem. – Eur. J.*, 2021, **27**, 16260–16269.
32 W. Leis, M. A. Argüello Cordero, S. Lochbrunner, H. Schubert and A. Berkefeld, A Photoreactive Iron(II) Complex Luminophore, *J. Am. Chem. Soc.*, 2022, **144**, 1169–1173.
33 S. Mukherjee, D. E. Torres and E. Jakubikova, HOMO inversion as a strategy for improving the light-absorption properties of Fe(II) chromophores, *Chem. Sci.*, 2017, **8**, 8115–8126.
34 J. D. Braun, I. B. Lozada, C. Kolodziej, C. Burda, K. M. E. Newman, J. van Lierop, R. L. Davis and D. E. Herbert, Iron(II) coordination complexes with panchromatic absorption and nanosecond charge-transfer excited state lifetimes, *Nat. Chem.*, 2019, **11**, 1144–1150.
35 J. D. Braun, I. B. Lozada and D. E. Herbert, In Pursuit of Panchromatic Absorption in Metal Coordination Complexes: Experimental Delineation of the HOMO Inversion Model Using Pseudo-Octahedral Complexes of Diarylamido Ligands, *Inorg. Chem.*, 2020, **59**, 17746–17757.
36 K. Kunnus, M. Vacher, T. C. B. Harlang, K. S. Kjær, K. Haldrup, E. Biasin, T. B. van Driel, M. Pápai, P. Chabera, Y. Liu, H. Tatsuno, C. Timm, E. Källman, M. Delcey, R. W. Hartsock, M. E. Reinhard, S. Koroidov, M. G. Laursen, F. B. Hansen, P. Vester, M. Christensen,

L. Sandberg, Z. Németh, D. S. Szemes, É. Bajnóczi, R. Alonso-Mori, J. M. Glownia, S. Nelson, M. Sikorski, D. Sokaras, H. T. Lemke, S. E. Canton, K. B. Møller, M. M. Nielsen, G. Vankó, K. Wärnmark, V. Sundström, P. Persson, M. Lundberg, J. Uhlig and K. J. Gaffney, Vibrational wavepacket dynamics in Fe carbene photosensitizer determined with femtosecond X-ray emission and scattering, *Nat. Commun.*, 2020, **11**, 634.

37 S. Alesi, F. Di Maria, M. Melucci, D. J. Macquarrie, R. Luque and G. Barbarella, Microwave-assisted synthesis of oligothiophene semiconductors in aqueous media using silica and chitosan supported Pd catalysts, *Green Chem.*, 2008, **10**, 517–523.

38 J. K. Lee, H. S. Kim and S. J. Yun, Synthesis of organic dye containing an alkylenesulfanyl-bridged bithienyl π-linker and its use in dye-sensitized solar cells, *J. Photochem. Photobiol., A*, 2014, **275**, 47–53.

39 I. H. M. van Stokkum, D. S. Larsen and R. van Grondelle, Global and target analysis of time-resolved spectra, *Biochim. Biophys. Acta, Bioenerg.*, 2004, **1657**, 82–104.

40 J. J. Snellenburg, S. P. Laptenok, R. Seger, K. M. Mullen and I. H. M. van Stokkum, Glotaran: A Java-Based Graphical User Interface for the R Package TIMP, *J. Stat. Softw.*, 2012, **49**(3), 1–22.

41 T. Duchanois, T. Etienne, C. Cebrián, L. Liu, A. Monari, M. Beley, X. Assfeld, S. Haacke and P. C. Gros, An Iron–Based Photosensitizer with Extended Excited–State Lifetime: Photophysical and Photovoltaic Properties, *Eur. J. Inorg. Chem.*, 2015, **2015**, 2469–2477.

42 C. Cebrián, M. Pastore, A. Monari, X. Assfeld, P. C. Gros and S. Haacke, Ultrafast Spectroscopy of Fe(II) Complexes Designed for Solar–Energy Conversion: Current Status and Open Questions, *ChemPhysChem*, 2022, **23**(7), e202100659.

43 F. Hainer, N. Alagna, A. Reddy Marri, T. J. Penfold, P. C. Gros, S. Haacke and T. Buckup, Vibrational Coherence Spectroscopy Identifies Ultrafast Branching in an Iron(II) Sensitizer, *J. Phys. Chem. Lett.*, 2021, **12**, 8560–8565.

44 P. Zimmer, L. Burkhardt, A. Friedrich, J. Steube, A. Neuba, R. Schepper, P. Müller, U. Flörke, M. Huber, S. Lochbrunner and M. Bauer, The Connection between NHC Ligand Count and Photophysical Properties in Fe(II) Photosensitizers: An Experimental Study, *Inorg. Chem.*, 2018, **57**, 360–373.

45 H. Tatsuno, K. S. Kjær, K. Kunnus, T. C. B. Harlang, C. Timm, M. Guo, P. Chàbera, L. A. Fredin, R. W. Hartsock, M. E. Reinhard, S. Koroidov, L. Li, A. A. Cordones, O. Gordivska, O. Prakash, Y. Liu, M. G. Laursen, E. Biasin, F. B. Hansen, P. Vester, M. Christensen, K. Haldrup, Z. Németh, D. Sárosiné Szemes, É. Bajnóczi, G. Vankó, T. B. Van Driel, R. Alonso-Mori, J. M. Glownia, S. Nelson, M. Sikorski, H. T. Lemke, D. Sokaras, S. E. Canton, A. O. Dohn, K. B. Møller, M. M. Nielsen, K. J. Gaffney, K. Wärnmark, V. Sundström, P. Persson and J. Uhlig, Hot Branching Dynamics in a Light–Harvesting Iron Carbene Complex Revealed by Ultrafast X–ray Emission Spectroscopy, *Angew. Chem., Int. Ed.*, 2020, **59**, 364–372.

46 R. A. Marcus, On the Theory of Oxidation–Reduction Reactions Involving Electron Transfer. I, *J. Chem. Phys.*, 1956, **24**, 966–978.

47 K. S. Kjær, K. Kunnus, T. C. B. Harlang, T. B. Van Driel, K. Ledbetter, R. W. Hartsock, M. E. Reinhard, S. Koroidov, L. Li, M. G. Laursen, E. Biasin, F. B. Hansen, P. Vester, M. Christensen, K. Haldrup, M. M. Nielsen, P. Chabera, Y. Liu, H. Tatsuno, C. Timm, J. Uhlig, V. Sundstöm, Z. Németh, D. S. Szemes, É. Bajnóczi, G. Vankó, R. Alonso-Mori, J. M. Glownia, S. Nelson, M. Sikorski, D. Sokaras, H. T. Lemke, S. E. Canton, K. Wärnmark, P. Persson, A. A. Cordones and K. J. Gaffney, Solvent control of charge transfer excited state relaxation pathways in [Fe(2,2′-bipyridine)$(CN)_4$, *Phys. Chem. Chem. Phys.*, 2018, **20**, 4238–4249.

48 M. Reiher, O. Salomon and B. A. Hess, Reparameterization of hybrid functionals based on energy differences of states of different multiplicity, *Theor. Chem. Acc.*, 2001, **107**, 48–55.

49 F. Weigend, Accurate Coulomb-fitting basis sets for H to Rn, *Phys. Chem. Chem. Phys.*, 2006, **8**, 1057.

50 F. Neese, Software update: The ORCA program system—Version 5.0, *Wiley Interdiscip. Rev.: Comput. Mol. Sci.*, 2022, **12**, e1606.

51 S. Hirata and M. Head-Gordon, Time-dependent density functional theory within the Tamm–Dancoff approximation, *Chem. Phys. Lett.*, 1999, **314**, 291–299.

52 T. Roland, J. Léonard, G. Hernandez Ramirez, S. Méry, O. Yurchenko, S. Ludwigs and S. Haacke, Sub-100 fs charge transfer in a novel donor–acceptor–donor triad organized in a smectic film, *Phys. Chem. Chem. Phys.*, 2012, **14**, 273–279.

53 L. Liu, P. Eisenbrandt, T. Roland, M. Polkehn, P.-O. Schwartz, K. Bruchlos, B. Omiecienski, S. Ludwigs, N. Leclerc, E. Zaborova, J. Léonard, S. Méry, I. Burghardt and S. Haacke, Controlling charge separation and recombination by chemical design in donor–acceptor dyads, *Phys. Chem. Chem. Phys.*, 2016, **18**, 18536–18548.